PROCEEDINGS OF SCIENCE

QCD and top phenomena at future colliders

Stefan Kluth[a,*]

[a] *Max-Planck-Institut für Physik,*
Boltzmannstr. 8, 85748 Garching, Germany

E-mail: skluth@mpp.mpg.de

In this review we summarise expectations for measurements of QCD observables and top quark properties from studies performed for proposed future collider projects.

Corfu2023 Workshop on future accelerators
25.04.2023
Corfu

*Speaker

https://pos.sissa.it/

PoS(CORFU2023)013

1. Introduction

The scope of this contribution to the Corfu2023 workshop on future colliders is on overview of topics of Quantum Chromo Dynamics (QCD) and some top quark properties, for which significantly improved measurements are expected with currently discussed future colliders. The selection of topics concentrates mostly on well-documented cases [1], but of course remains a subjective choice and all omissions are the fault of the author.

As future projects we consider as a main guideline the FCC program proposed by CERN [2] consisting of a new circular tunnel in the Geneva area of about 100 km circumference, with a new electron-positron collider FCC-ee as a first stage. In a second stage a new hadron collider FCC-hh is foreseen with proton-proton collisions energies of up to 100 TeV. The FCC-ee is designed to reach a maximal collision energy of 365 GeV which covers the production thresholds of all heavy bosons of the standard model (W-, Z-, Higgs-boson) with very large luminosity and the production threshold for top quark pairs.

Other project proposals are the CEPC in China [3, 4], which is similar in scope to the CERN FCC program, the ILC in Japan [5], which as a linear electron-positron collider would be capable of reaching beyond 500 GeV centre-of-mass (cms) energies.

The Large Hadron Electron Collider (LHeC) proposes to add a high luminosity electron accelerator with beam energies of about 50 GeV to the existing LHC complex in order to reach electron-proton cms energies of about 1.3 TeV [6]. The large cms energy enables the production of all heavy bosons and fermions of the standard model in deep inelastic scattering (DIS).

For studies of QCD, as projected onto determinations of the strong coupling constant $\alpha_s(m_Z)$, the expected very large data samples of the FCC-ee program would be transformative. Currently the expected samples are $3 \cdot 10^{12}$ hadronic Z boson decays, including $6 \cdot 10^{11}$ Z boson decays to b quarks, 10^{11} Z boson decays to τ lepton pairs, $5 \cdot 10^8$ W boson decays as well as 10^6 $t\bar{t}$ events at the production threshold.

2. Top quark properties

The main impact on the measurements of top quark properties is arguably the expected precision of the top quark mass and width, which could be achieved with a scan of the cross section of $t\bar{t}$ production in e^+e^- annihilation around the threshold cms energy of $\sqrt{s} \approx 343$ GeV.

This is illustrated in figure 1 [2, 7]. Figure 1 (left) shows QCD predictions for the cross section with 3-loop corrections (N3LO) as a function of the cms energy $\sqrt{s}$ in different scenarios. The "LS" scenario refers to the influence of the luminosity spectrum expected at the FCC-ee at these $\sqrt{s}$, i.e. the changes to $\sqrt{s}$ induced by the interaction of the two beams with each other. The "ISR" scenario refers to the influence of initial state photon radiation from the beam particles on $\sqrt{s}$. The arrows with labels indicate the sensitivity of the cross section shape to changes of parameters of the predictions $(m_t, \Gamma_t, \alpha_s, y_t)$. The LS spectrum as well as the ISR effects will broaden and smear the threshold shape but the effects of ISR are expected to be larger compared to the LS effects. Figure 1 (right) presents the realistic default prediction with LS and ISR effects while the shaded bands correspond to variations of m_t or Γ_t in the predictions. The sensitivity of the cross section shape to these parameters is distributed differently over $\sqrt{s}$.

Results from these simulation studies are $m_t = (171.5 \pm 0.017_{stat.} \pm 0.007_{cms} \pm 0.005_{\alpha_s} \pm 0.040_{theo.})$ GeV and $\Gamma_t = (1.37 \pm 0.045_{stat.} \pm 0.003_{cms} \pm 0.005_{\alpha_s} \pm 0.040_{theo.})$ GeV. According to these studies measurements of the top quark mass and width will be possible with uncertainties well below 100 MeV, which would correspond to a reduction of the uncertainties by a factor of O(10) w.r.t. to current best measurements [8]. In addition, the inclusive nature of the total cross section enables unambigous theory predictions directly in terms of parameters of the theory in a known renormalisation scheme, in contrast to the currently best determinations based on top quark decays and predictions obtained with Monte Carlo simulations, see e.g. [9].

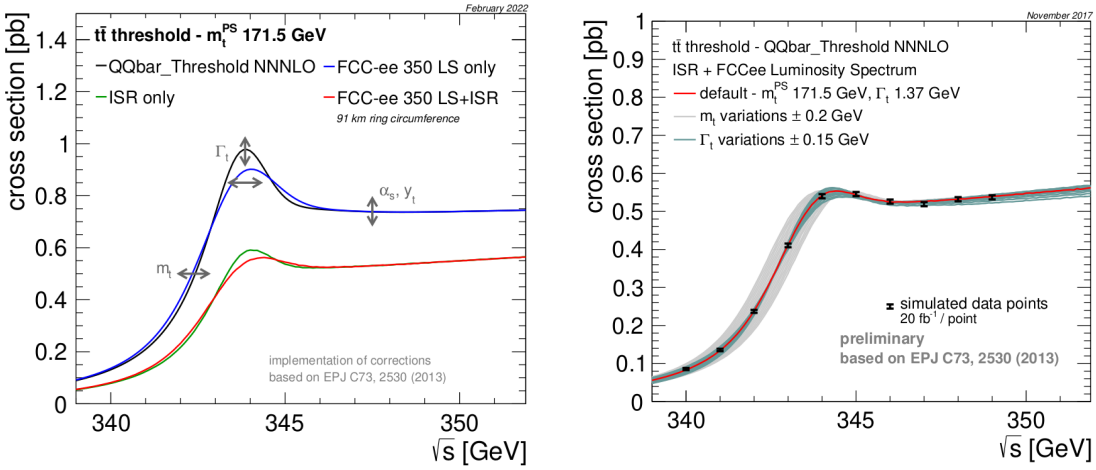

Figure 1: (left) The predicted cross section for $t\bar{t}$ production in e^+e^- annihilation as a function of cms energy $\sqrt{s}$ is shown. The lines with different colours show changes induced by considering effects of the beam luminosity spectrum (LS) and initial state radiation (ISR). The arrows indicate sensitivity of the predictions to top quark properties. (right) The figure shows simulated data points for the $t\bar{t}$ production cross section in e^+e^- annihilation, and superimposed the prediction with parameters indicated on the figure [2, 7].

3. Z and W boson decays

The sensitivity of hadronic Z or W boson decays to the strong coupling is connected with QCD radiative corrections to the electro-weak Feynman diagrams of these decays. In the case of the Z boson this is well studied and documented [10]. The measurements of production cross sections and branching fractions for decays to hadrons or leptons are translated into the relevant quantities called "Electroweak precision observables" EWPO. For determinations of the strong coupling constant the most sensitive observable is the ratio of the hadronic and leptonic branching fractions $R_l^{Z(W)}$ for Z (W) bosons. The prediction can be written (see e.g. [1]) for Z (W) bosons as

$$R_l^{Z(W)} = \Gamma_{had.}/\Gamma_{lept.} = R_{ew}\left(1 + \sum_{i=1}^{3} a_i \left(\frac{\alpha_s(Q)}{\pi}\right)^i + \delta_{ew} + \delta_{mix} + \delta_{np}\right) \quad , \tag{1}$$

where R_{ew} accounts for the prediction from electro-weak theory, a_i are fixed order coefficients from the QCD corrections, $\alpha_s(Q)$ is the strong coupling evaluated at scale Q, δ_{ew} contains electo-weak corrections, δ_{mix} contains mixed electro-weak and QCD corrections and δ_{np} contains non-perturbative corrections.

A recent analysis [1] of this relation and other observables sensitive to QCD corrections in the electro-weak theory together with LEP Z boson EWPO corrected for improved determination of the luminosity yields $\alpha_s(m_Z) = 0.120 \pm 0.003_{exp.} \pm 0.001_{theo.}$. In the same work the analysis of the branching ratios of the W boson yields $\alpha_s(m_Z) = 0.107 \pm 0.035_{exp.} \pm 0.002_{theo.}$.

In the programs of new e^+e^- colliders the measurements of Z boson EWPO, the W boson pair production cross section at threshold and the Z and W boson branching ratios are expected to improve significantly, see e.g. [2], tab.3.1. The experimental uncertainty on the strong coupling $\alpha_s(m_Z)$ was determined to be much smaller than the current theoretical uncertainty based on N3LO QCD predictions, and the available electro-weak and mixed corrections. In addition, for a determination of $\alpha_s(m_Z)$ from the W boson data improved measurements of the CKM mixing matrix are necessary.

Assuming that electro-weak corrections of $O(\alpha^2)$, $O(\alpha^3)$, 4-loop QCD corrections (N4LO), and the mixed corrections of $O(\alpha\alpha_s^2)$, $O(\alpha\alpha_s^3)$ and $O(\alpha^2\alpha_s)$ will be available, the following measurements of the strong coupling from Z and W boson EWPO could be achieved [1]:

$$\begin{aligned} Z : \alpha_s(m_Z) &= 0.12020 \pm 0.00013_{exp.} \pm 0.00005_{par.} \pm 0.00022_{theo.} \\ W : \alpha_s(m_Z) &= 0.11790 \pm 0.00012_{exp.} \pm 0.00004_{par.} \pm 0.00019_{theo.} \end{aligned}$$

These results are illustrated in figure 2. Figure 2 shows for Z (left) and W (right) bosons the dependence on $\alpha_s(m_Z)$ of the $\Delta\chi^2$ of fits of the complete theory prediction to data from LEP or simulated data from FCC-ee. The large improvement of the uncertainties is clearly visible.

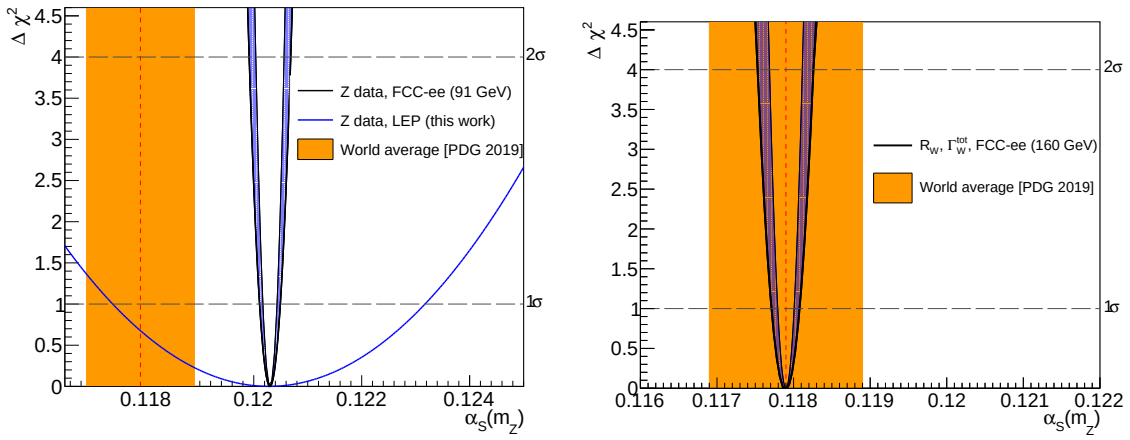

Figure 2: (left) The figure shows $\Delta\chi^2$ from fits to EWPO as function of $\alpha_s(m_Z)$. The light blue line corresponds to an updated fit to the LEP data while the dark blue area is the result of an extrapolation to EWPO measurements predicted for FCC-ee. (right) The figure shows with the dark blue area a prediction for $\Delta\chi^2$ based on EWPO for W boson properties from FCC-ee [1].

4. Fragmentation functions

The fragmentation function in hadronic final states of high energy collisions is constructed from particle momenta scaled to the energy scale of the hard scattering process. In the experiments

generally charged particles only are measured since low momentum particles dominate and at low energies momenta from charged particle tracks can be measured with much better precision compared with calorimeter based energy measurements needed for neutral particles. For hadronic final states in e^+e^- annihilation the scale in given by one half of the cms energy $\sqrt{s}/2$ while in DIS the invariant mass Q^2 of the 4-momentum transfer is used. In hadron collisions fragmentation functions are studied in central di-jet systems and the scale is given by the jet energy E_{jet} for the particles contained in one of the two jets.

4.1 Fragmentation functions in e^+e^- collisions at large x

In hadronic final states in e^+e^- annihilation the spectrum of scaled particle momenta $x_p = 2p/\sqrt{s}$ can be described as a convolution of a non-perturbative fragmentation function (FF) $D_f^h(x,\mu)$ and perturbative coefficient functions (CF) $C_f(x,\alpha_s(Q)$. The FFs corresponds to the distribution of hadrons h generated by a parton $f = u, d, s, c, b, g$ at scale μ. The CFs describe the probability to produce a parton f in the hard interaction. Taken together the cross section for producing hadrons is written as

$$\frac{1}{\sigma}\frac{d\sigma^h}{dx} = \sum_f \int_x^1 C_f\left(z,\alpha_s(Q)\right) D_f^h\left(\frac{x}{z},\mu\right)\frac{dz}{z} \quad . \tag{2}$$

The FF cannot be predicted directly in QCD since they describe the non-perturbative transition of partons to hadrons, but their scale dependence, i.e. the evolution of the $D_f^h(x,\mu)$ with scale μ is predicted in QCD by the DGLAP equations known up to NNLO. The CF are known in QCD in NNLO (see e.g. the review "Fragmentation Functions in e^+e^-, ep, and pp Collisions" [8]).

Figure 3 shows as an example measurements of charged particle momentum spectra as functions of cms energy $\sqrt{s}$ and x_p by OPAL and other experiments [11]. The solid lines show the result of a fit in NLO QCD with $\alpha_s(Q)$ as a free parameter and parametrised FFs at a reference scale. Non-perturbative effects are mostly captured by the FF and other non-perturbative corrections scale as $1/Q^2$. An average of comparable analyses by the LEP collaborations ALEPH, DELPHI and OPAL in [12] results in $\alpha_s(m_Z) = 0.1192 \pm 0.0056_{exp.} \pm 0.0070_{theo.}$.

An extrapolation of such analyses to data sets from future e^+e^- colliders remains speculative. With much larger data sets at high energies $\sqrt{s} > m_Z$ and much improved detectors allowing a better separation of signal and backgrounds it seems safe to expect $\Delta\alpha_s(m_Z)_{exp.} < 1\%$. Assuming that DGLAP evolution is available up to N3LO a theory uncertainty of $\Delta\alpha_s(m_Z)_{theo.} \approx 1\%$ might be possible.

4.2 Fragmentation functions at small x

Based on the same scaled momentum $x_p = 2p/\sqrt{s}$ in e^+e^- annihilation or $x_p = p/Q$ in DIS in the Breit frame, the quantity $\xi = \log(1/x_p)$ is defined in order to study the distribution of the dominant low momentum particles. The distribution is sensitive to QCD coherence effects for multiple soft gluon emission [13] with the consequence that the distribution is dominated by radiation corresponding to medium momenta. Figure 4 (left) shows a collection of data for scaled momentum spectra measured by several experiments in e^+e^- annihilation at cms energies from $\sqrt{s}$ = 2.2 to 206 GeV [1].

The approximate Gaussian shape of the distributions can be described with the distorted Gaussian model [14]. The FF after a Mellin transform $D_f^h(Q)$ with scale Q is approximated

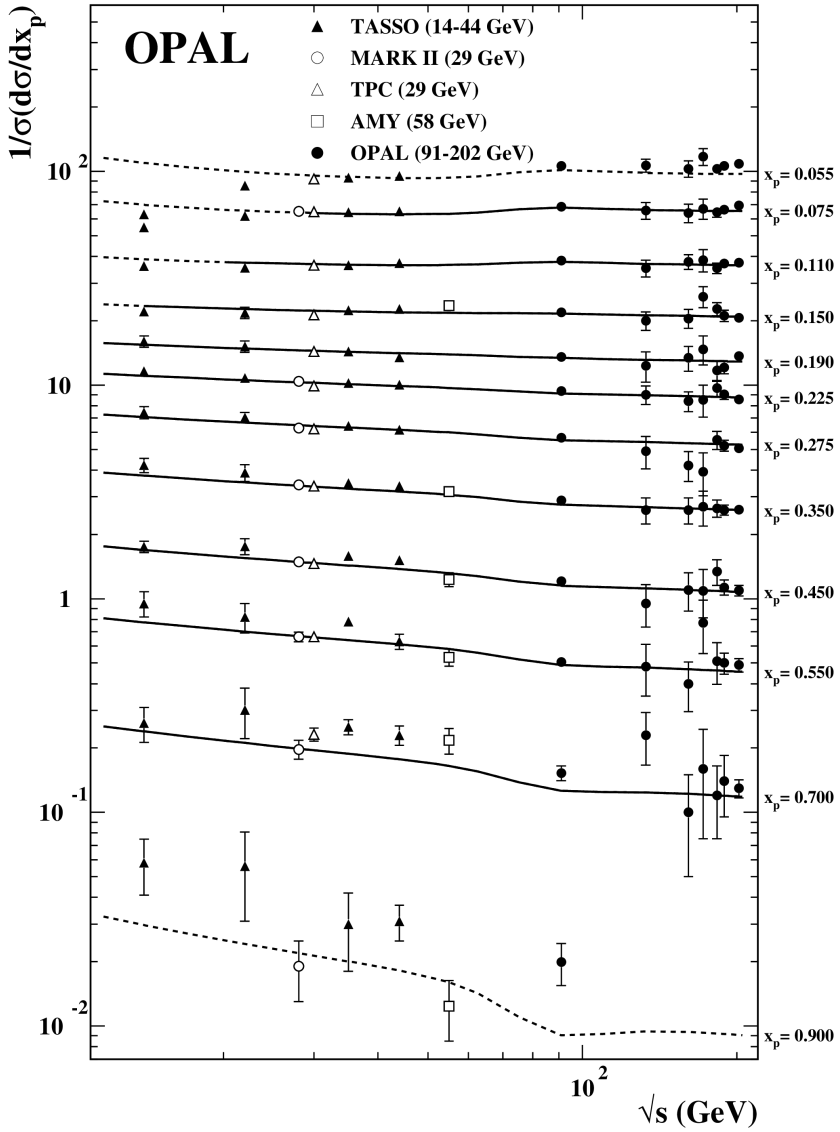

Figure 3: The figure shows the normalised cross sections for charged hadron production e^+e^- annihilation as function of cms energy $\sqrt{s}$ by OPAL and other experiments. The data points are binned in x_p as indicated. The lines show the result of a fit of the theory fit to the data (full) and extrapolations (dashed) [11].

with $D \approx C(\alpha_s(t))\exp(\int^t \gamma(\alpha_s(t'))dt')$ and $t = \log(Q)$. The anomalous dimension γ expands in integer and half-integer powers of α_s: $\gamma \sim O(\alpha_s^{1/2}) + O(\alpha_s^1) + O(\alpha_s^{3/2}) + O(\alpha_s^2) + \ldots$. The integer powers of α_s are associated with fixed order corrections while the half-integer powers are due to resummation of soft and collinear logarithms. In momentum space evolution equations for moments (e.g. the peak position ξ_0) are derived, which allow a determination of the strong coupling α_s [1] by applying this formalism e.g. to the peak positions of the data shown in figure 4 (left). These peak positions are shown together with more measurements from DIS in figure 4 (right). The dashed line shows the result of a fit to the evolution equations in NNLO*+NNLL[1]. The result

[1]NNLO* refers to a partial calculation of the NNLO corrections.

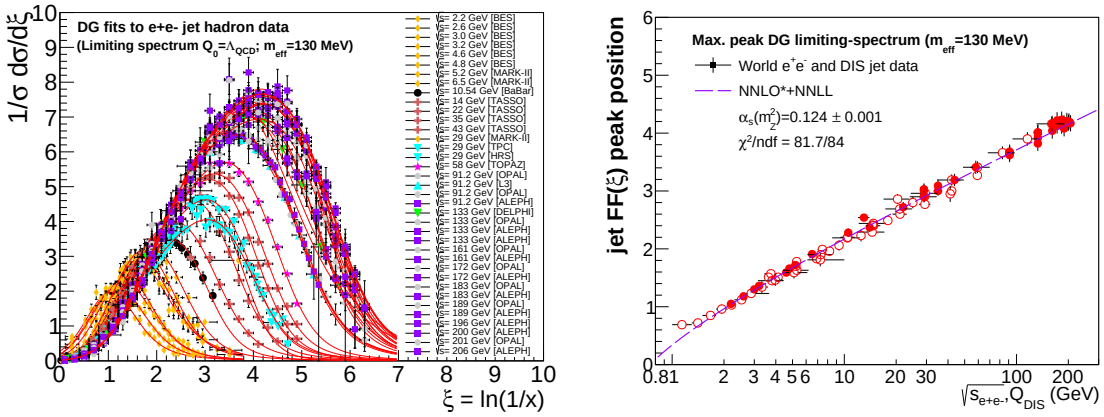

Figure 4: (left) The figure shows normalised cross sections for charged hadron production in e^+e^- annhilation as function of $\xi = \log(1/x)$ by various experiments as indicated. Superimposed are fits of distorted gaussian (DG). (right) The figure shows the peak position obtained from DG fits as function of cms energy $\sqrt{s}$ (full points e^+e^-) or Q_{DIS} (open points DIS). Superimposed is the fitted QCD prediction as indicated [1].

of a simultaneous analysis of the peak position and the charged particle multiplicity evolution is $\alpha_s(m_Z) = 0.121 \pm 0.001_{exp.} \pm 0.002_{theo.}$.

Measurements of fragmentation functions in $p\bar{p}$ collisions at $\sqrt{s} = 1.8$ TeV have been performed by CDF [15]. The charged particle momenta are normalised by the energy of the jet containing the particle h in question such that $x = E_h/E_{jet}$ and $\xi = \log(1/x)$. The charged particles are restricted to be within a cone of opening angle θ_c around the jet axis. The overall scale of of the di-jet system is given by its invariant mass M_{jj}. Figure 5 (left) shows distributions of ξ in bins of M_{jj} measured by CDF [15]. It is clearly visible that the shape of the distributions is similar to those from e^+e^- annihilation shown in figure 4 (left), and that the peak positions increase in ξ with increasing M_{jj}.

With these variables and scales the distributions of ξ in bins of $Q_{jj} = M_{jj} \sin\theta_c$ are subject to the same theoretical treatment as described above [15]. Figure 5 (right) presents the peak positions as function of scale Q_{jj} for three different values of the cone opening angle θ_c. In addition the figure shows data from e^+e^- annihilation and DIS scaled to the relevant opening angle $\theta_c = \pi/2 \approx 1.57$. The line on figure 5 (right) corresponds to a fit of a more simple theory approximation to the CDF data points.

The FF at small x has also been studied for heavy quarks. Gluon radiation from heavy quarks is influenced by the "dead cone" effect [16, 17]. Radiation from an energetic, but not ultra-relativistic, heavy quark Q with energy E_Q, mass M_Q and $E_Q/M_Q \gg 1$ is suppressed at small angles $\theta < \theta_0 = E_Q/M_Q$ and large energies ω according to

$$d\sigma_{Q\to Q+g} \simeq \frac{\alpha_s}{\pi} C_F \frac{\theta^2 d\theta^2}{(\theta^2+\theta_0^2)^2} \frac{d\omega}{\omega} \quad , \tag{3}$$

$C_F = 4/3$ is the QCD colour factor at the branching vertex $Q \to Q + g$. The main consequence for the FF of heavy quarks is the suppression of particles with large x [16].

The measurements by DELPHI and OPAL of the heavy quark FF as a function of $\xi = \log(1/x)$ with Z boson decays to b and c quark pairs where analysed in [18]. Since the measurements of charged particle momenta by DELPHI and OPAL also contain the charged decay products of B-

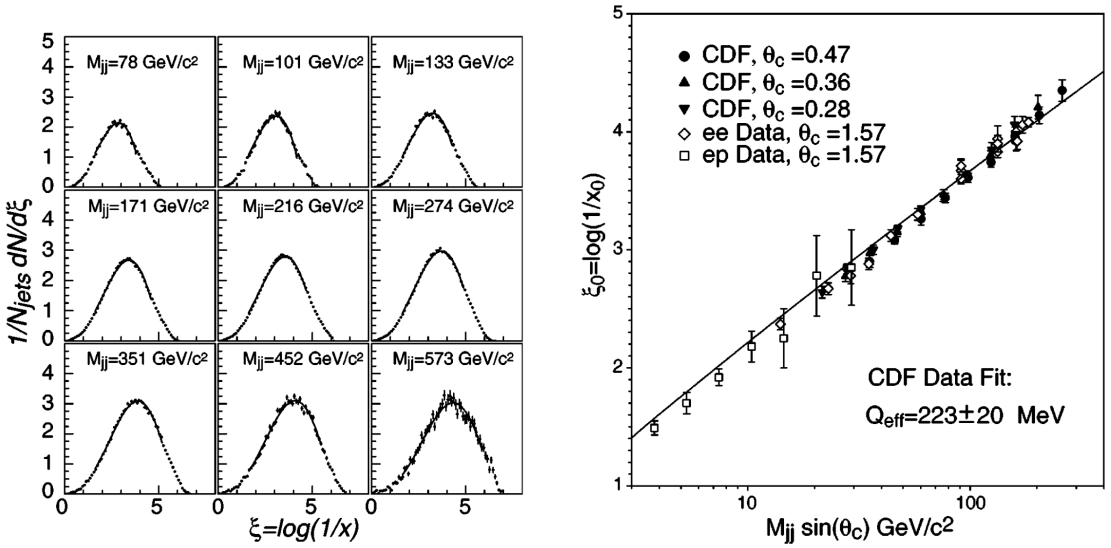

Figure 5: (left) The figure shows measurements by CDF of charged particle momentum spectra as function of $\xi = \log(1/x)$ in cone jets with opening angle $\sin\theta_c = 0.36$ in bins of di-jet invariant mass M_{jj}. Superimposed are fits to determine the peak position. (right) The figure shows the peak positions extracted from spectra of different cone jet sizes as indicated together with data from e^+e^- annihilation and DIS (ep) as function of scale parameter $M_{jj}\sin\theta_C$. Superimposed is the result of a fit by CDF (full line) [15].

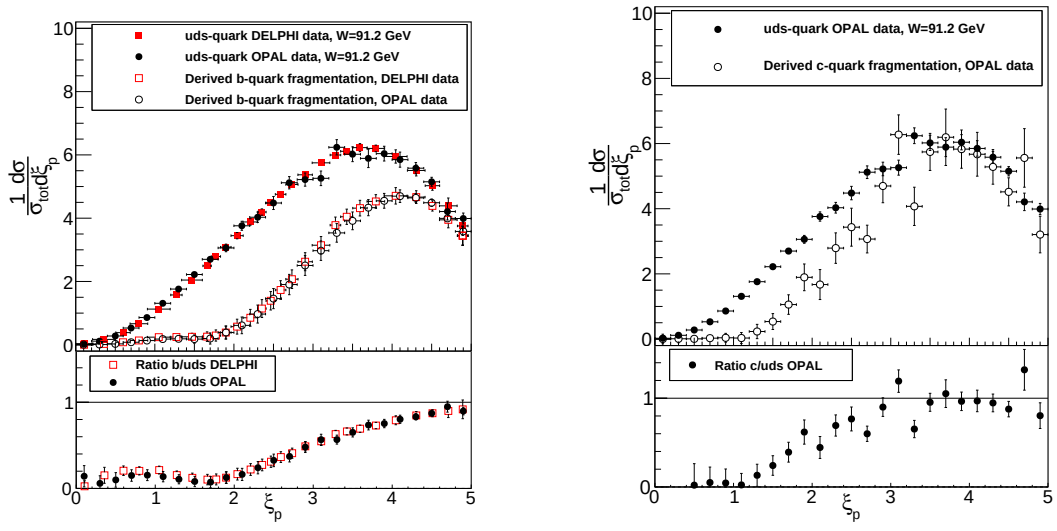

Figure 6: (left) The figure shows charged particle momentum spectra for Z boson decays to light (uds) and b quarks after correction for B hadron decay products based on DELPHI and OPAL data. (right) The same as (left) for c quarks based on OPAL data. For both figures the lower plots present the ratios of FFs for heavy and light quarks as indicated [18].

or Charm-hadrons their contribution is subtracted using simulated Z boson decays. The results are shown in figure 6 for b quarks (left) and c quarks (right). The open points display the FF of the heavy quark after subtraction of the heavy hadron decay contribution. The solid points show the FF for light quarks (u,d,s). The strong suppression of the heavy quark FFs at small ξ (large x) is clearly visible.

With new e^+e^- colliders such as FCC-ee with very large data samples at $\sqrt{s} = m_Z$ and high $\sqrt{s} > m_Z$ a reduction of $\Delta\alpha_{S,exp.} < 1\%$ for extraction of α_s from evolution of the FF at small x are expected. In order to reduce the then dominant theory uncertainty progress in the accuracy of the predictions is required [1].

Measurements of the FF at small x in hadron collisions as presented by CDF [15] (see above) with data from LHC experiments and in the future at a possible hadron collider as part of the FCC program (FCC-hh) could extend the scales probed in the evolution to $M_{jj} \sin\theta_c = \mathrm{O(TeV)}$. It remains to be studied what the expected uncertainties of an extraction of α_s from the evolution of moments of the distributions would be.

The measurement of the FF from heavy quarks (c, b, top) at future e^+e^- colliders would also substantially improve upon existing analysis due to much larger event samples and substantially improved detectors. Such measurements could give access to heavy quark masses [18], and possibly to the width of the top quark [19].

5. Jets and event shapes

Hadronic final states of high energy collisions can studied with jet clustering algorithms or event shape observables. The general idea is to quantify the topology of the event, i.e. the presence of one or more collimated bundles of particles (see e.g. [12, 20]). Jet clustering algorithms perform physically motivated clustering of particles close in phase space. The distance between objects is e.g. defined as the invariant mass of a pair of objects. In hierarchical clustering, at each step the pair of objects with the smallest distance is merged, usually by adding their 4-vectors. The objects are removed from the list of objects and the merged object is added.

In order to define an event shape observable all objects of the event are used to calculate a measure corresponding to the event topology. The thrust observable τ is given by $T = \max_{\vec{n}}(\sum_i |\vec{p}_i \cdot \vec{n}|/\sum_i |\vec{p}_i|)$ and $\tau = 1 - T$. The value of τ is small for collimated 2-jet like events while it increases if more jet activity is present.

For a meaningful comparison of measurements with theory predictions the observables have to "infrared-collinear safe" (IRC safe). The concept is that small changes in the event topology due to fluctuations in the parton shower cascade or due to the transition from partons to hadrons should only change the observable value by a small amount such that the interpretation of an event does not change [21].

For jet and event shape observables in hadronic final states with 2- and 3-jet like topologies in e^+e^- annihilation QCD predictions in NNLO exist since many years. The prediction for the normalised cross section can be shown simplified for a generic observable y as:

$$\frac{1}{\sigma_{tot}}\frac{d\sigma}{dy} = \alpha_s(Q)\frac{dA}{dy} + \alpha_s^2(Q)\frac{dB}{dy} + \alpha_s^3(Q)\frac{dC}{dy} + h.o. + s.d. + \sigma_0 \to \sigma_{tot.} \quad . \tag{4}$$

Terms connected with higher order corrections (h.o.), dependence on the renormalisation scale (s.d.) and the correction for the total hadronic cross section $\sigma_{tot.} = \sigma_0(1 + \alpha_s/\pi + h.o.)$ are not shown. The coefficient functions dA/dy etc. are generally calculated by numerically integrating the corresponding QCD matrix elements with Monte Carlo methods [22–24].

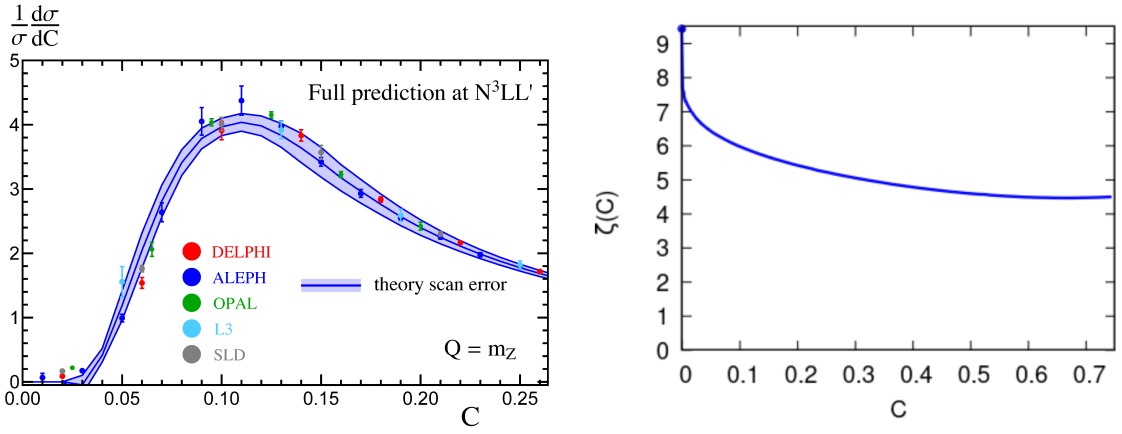

Figure 7: (left) The figure shows the distribution of the C-parameter measured with hadronic Z boson decays by several experiments as indicated. Superimposed as line and band is the QCD prediction with theory uncertainty [25]. (right) The figure shows the function $\zeta(C)$ corresponding to the observable dependent non-perturbative corrections from [26], see text for details.

The most complete predictions for event shape observables thrust (τ) and C-parameter ($C = 3/2 \sum_{ij} |\vec{p}_i||\vec{p}_j| \sin^2\theta_{ij}/(\sum_i |\vec{p}_i|)^2$) were shown in [25], including resummation at approximate N3LL accuracy and an analytic model for non-perturbative corrections. The results for the strong coupling are

$$\begin{aligned} \tau : \alpha_s(m_Z) &= 0.1134 \pm 0.0002_{exp.} \pm 0.0005_{had.} \pm 0.0011_{theo.} \\ C : \alpha_s(m_Z) &= 0.1123 \pm 0.0002_{exp.} \pm 0.0007_{had.} \pm 0.0014_{theo.} \end{aligned} \quad (5)$$

The analysis was recently confirmed [27] and investigated for systematic effects in the non-perturbative model and in the setting of the renormalisation scale in the QCD predictions. The measurements are in tension with most other measurements of the strong coupling and thus the world average. The study [27] finds some deviations which are larger than the quoted uncertainties. In [25] it was observed that the choice of model for non-perturbative corrections can lead to $\Delta\alpha_s(m_Z)_{non-pert.} = O(1)\%$ while [26] explored a more realistic analytic non-perturbative model which takes 3-jet topologies into account.

Figure 7 (left) [25] shows the region of small values of C with data from various experiments and the complete theory prediction as shaded band. The good description of the data by the prediction is evident. The agreement between data and theory is also good in regions of larger values of C. Figure 7 (right) [26] shows a function $\zeta(C)$ which according to the model of [26] gives the correction due to non-perturbative effects. The main conclusion is that the non-perturbative corrections vary from small values of C (2-jet like topology) to large values of C (3 or more jets topology). In the study [26] this observation is found to explain some of the difference between the results for $\alpha_s(m_Z)$ in equation (5) and the world average.

Measurements of $\alpha_s(m_Z)$ with data from new e^+e^- colliders will profit from very large data samples at $\sqrt{s} = m_Z$ and above combined with proposed detector performance exceeding that of the LEP experiments by a large margin. The experimental uncertainty is projected as $\Delta\alpha_s(m_Z)_{exp.} < 0.1\%$. Other uncertainties are expected to be limited to be $\Delta\alpha_s(m_Z)_{had.} \approx 1\%$ and $\Delta\alpha_s(m_Z)_{theo.} \approx 1\%$, or less [1]. In addition in [26] the uncertainty from effects of finite hadron masses on the theory predictions was estimated as $\Delta\alpha_s(m_Z)_{hadron\,masses} \approx 1\%$.

Jet production in pp collisions at the LHC is an obvious and interesting observable. Single inclusive jet production for the LHC can be predicted in complete NNLO QCD [28]. The comparison to data from the experiments ATLAS and CMS proceeds via grids of such predictions as functions of α_s, renormalisation and factorisation scale settings and parton density function (pdf) sets [29]. A recent study [29] with approximated NNLO predictions estimated $\Delta\alpha_s(m_Z)_{theo.} \approx 1\%$ with experimental uncertainties of $\Delta\alpha_s(m_Z)_{exp.} = 1.1\%$.

Event shape observables for pp collisions are also a promising alternative for measurements of the strong coupling constant at high energies. An example is the recent measurement of the jet based transverse energy-energy correlation (TEEC) by ATLAS at $\sqrt{s} = 13$ GeV. Events are selected after clustering into anti-kt jets with $R = 0.4$, transverse momentum $p_t > 60$ GeV and pseudo-rapidity $|\eta| < 2.4$ if at least two jets are present and $H_{T2} = p_{t,1} + p_{t,2} > 1$ TeV. From the jets the TEEC is calculated as the distribution of pairwise azimuth angle differences weighted by the product of the transverse jet energies. The data are analysed in bins of H_{T2} between 1 TeV and more than 3.5 TeV. The experimental uncertainties are $\Delta\alpha_s(m_Z)_{exp.} < 1\%$ while combined theory uncertainties are $\Delta\alpha_s(m_Z)_{theo.} \approx 2\%$. Uncertainties from non-perturbative effects are $\Delta\alpha_s(m_Z)_{non-pert.} \approx 0.5\%$ due to the large energy scale H_{T2} of the jet production.

6. $\sqrt{s} < m_Z$

The potential of low energy ($\sqrt{s} < m_Z$) data from e^+e^- annihilation for studies of QCD is great, see e.g. [30]. Many current global fits of event shape observables (see above) include low energy data in order to disentangle perturbative and non-perturbative effects, which evolve differently with the energy scale $\sqrt{s}$. However, the data samples from the PETRA experiments or the other e^+e^- colliders before LEP are limited in size and also in measurement precision in comparison to current detector technologies.

New e^+e^- colliders and in particular the FCC-ee could enable to revisit physics at low annihilation energies[2]. Many of the measurements discussed in this report could be improved significantly with new low energy data. The main arguments are illustrated in figure 8. Figure 8 (left) shows the cross section for the production of various final states. The strong enhancement at the Z boson peak is clearly visible. At $\sqrt{s} < m_Z$ the cross sections increase with decreasing $\sqrt{s}$. Figure 8 (right) shows estimates for the luminosity of the FCC-ee and other proposed colliders. The FCC-ee luminosity increases steeply with decreasing $\sqrt{s}$. It is thus reasonable to expect that the FCC-ee could be operated at low energies with luminosities at the levels possible for the Z boson peak. If this expectation could be realised the collection of a sample of 10^9 events at cms energies between 20 and 40 GeV would be possible. The event production rate for a cross section of 10^3 pb at a

[2] www.snowmass21.org/docs/files/summaries/EF/SNOWMASS21-EF5_EF4_Andrii_Verbytskyi-208.pdf

luminosity of $4 \cdot 10^{36}/(cm^2 s)$ is 4000 events/s. This implies about 3 days of continuous machine operation would be needed to collect a sample of 10^9 events.

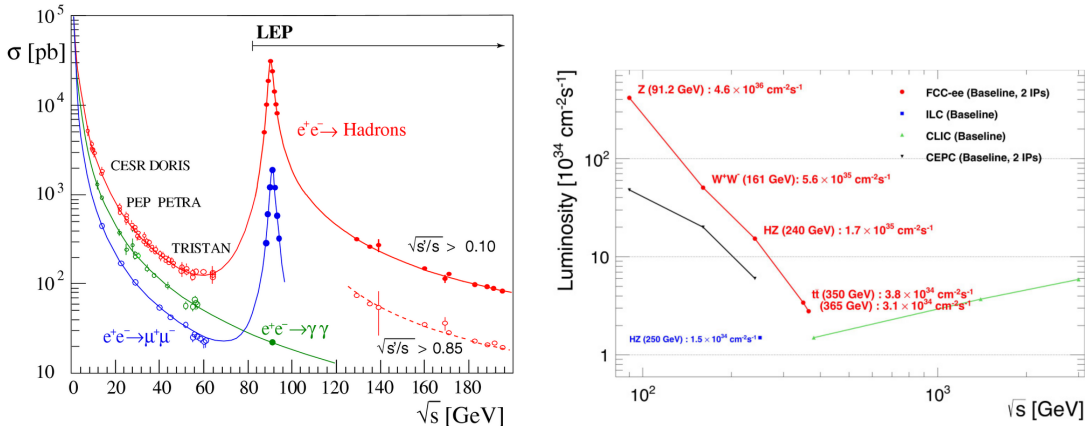

Figure 8: (left) The figure shows cross sections for production of various final states in e^+e^- annihilation as function of cms energy $\sqrt{s}$ as indicated. (right) The figure shows predictions for the luminosity of the FCC-ee (red) and other e^+e^- collider proposals at cms energy $\sqrt{s}$ [31].

The data collected by e.g. FCC-ee runs with $\sqrt{s} < m_Z$ could potentially be used for a precise determination of the strong coupling constant based on the "R-ratio" given by

$$R_l^\gamma(Q) = \frac{\sigma(e^+e^- \to hadrons)}{\sigma(e^+e^- \to \mu^+\mu^-)} = 3 \sum_i q_i^2 (1 + \alpha_s(Q)/\pi + \ldots) \qquad (6)$$

measured at a given cms energy $\sqrt{s} = Q$. In the SM prediction the q_i are the quark charges, and it is known up to N4LO, see e.g. [32]. With $dR_l^\gamma/d\alpha_s \approx 1$ for four or five quark flavours one gets the approximate relation $3\Delta R_l^\gamma/R_l^\gamma \approx \Delta\alpha_s(Q)$. Thus in order to achieve a statistical precision of 0.1% on $\alpha_s(m_Z)$ a relative error $\Delta R_l^\gamma/R_l^\gamma \approx 10^{-4}$ is needed. This corresponds to sample sizes of O(10^8) events. For the related EWPO $R_l^Z = \Gamma(Z \to hadrons)/\Gamma(Z \to \mu^+\mu^-)$ for Z boson decays for FCC-ee an experimental systematic uncertainty of $\Delta R_l^Z/R_l^Z \approx 5 \cdot 10^{-5}$ is estimated [2], which is dominated by uncertainties of the lepton acceptance of the detector. It seems reasonable to estimate a similar experimental uncertainty for the R-ratio R_l^γ at lower energies. Furthermore, the theory uncertainties for R_l^γ should be similar to those for $R_l^{Z(W)}$, i.e. about 0.2%, see section 3.

A different option for this kind of analysis would be using radiative hadronic Z boson decays $e^+e^- \to \gamma Z(\to hadrons)$ from the large sample of Z decays at FCC-ee. For example the OPAL collaboration used radiative hadronic Z boson decays to obtain measurements of α_s at low energies [33]. In this analysis based on $2.4 \cdot 10^6$ hadronic Z boson decays from 1560 (E_γ = 10 – 15 GeV) to 290 (E_γ = 40 – 45 GeV) radiative Z boson decays were selected for the ranges of photon energies E_γ in brackets. The sample sizes at FCC-ee are estimated to be larger by a factor of about 10^6 compared to the OPAL sample and thus they would also be of O(10^8).

7. Quark mass running

Quark masses are also free parameters of the theory of strong interactions, and are subject to evolution equations similar to the strong coupling constant α_s, see e.g. [34]. The quark masses are

predicted to decrease with increasing energy scale of a strong interaction with a heavy quark. In leading order in the $\overline{MS}$ scheme the running for the masses $m_q(\mu)$ for b and t quarks as a function of the energy scale μ is expressed as

$$m_b(\mu) = \hat{m}_b \left(\frac{\alpha_s(\mu)}{\pi}\right)^{12/23} , m_t(\mu) = \hat{m}_t \left(\frac{\alpha_s(\mu)}{\pi}\right)^{4/7} . \quad (7)$$

The $\hat{m}_q$ are reference masses. The quark mass running is predicted to be driven by the running of the strong coupling $\alpha_s(\mu)$. The different exponents for b and t quarks are due to different numbers of active quark flavours in the running.

The prediction of running quark masses has been tested for top quarks by CMS [35]. In the analysis top anti-top quark pair production in pp collisions at 13 TeV is studied as a function of the invariant masses of the top anti-top quark pairs $m_{t\bar{t}}$. Figure 9 (left) shows the measured differential cross section for top anti-top quark pair production in bins of $m_{t\bar{t}}$ corrected for experimental and hadronisation effects. Superimposed are QCD predictions in NLO for different values of the reference mass $m_t(m_t)$.

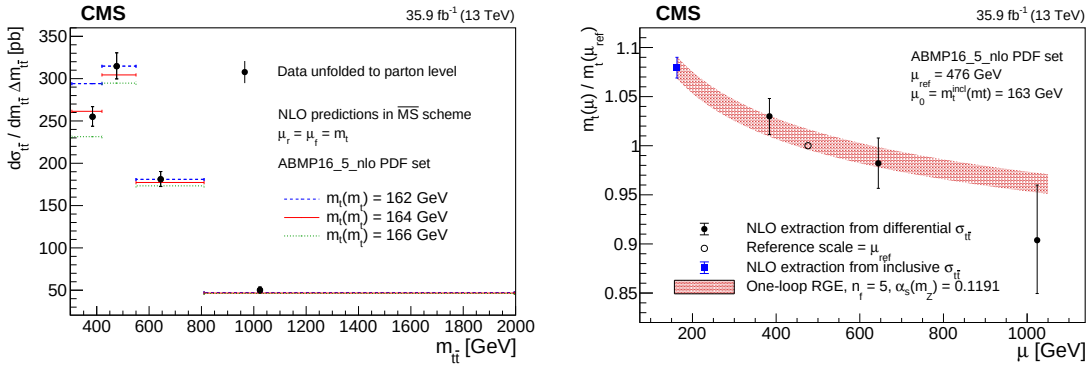

Figure 9: (left) The figure shows the cross section for $t\bar{t}$ production in pp collisions at 13 TeV in bins of $m_{t\bar{t}}$ measured by CMS. Superimposed are QCD predictions as function of the reference mass $m_t(m_t)$ as indicated. (right) The figure shows the ratios of extracted $m_t(\mu)$ to the reference value 476 GeV. The red band shows the LO QCD prediction for the running of the top quark mass with uncertainties [35].

The sensitivity of the predictions to $m_t(m_t)$ decreases with $m_{t\bar{t}}$. The invariant mass of the top quark pair can be written as $m^2_{t\bar{t}} \approx 2m^2_t + 2|p_t||p_{\bar{t}}|(1 - cos\theta_{t\bar{t}})$ for $p/m \gg 1$. Thus, for the last bin at $m_{t\bar{t}} \approx 1000$ GeV the first term $2m^2_t$ contributes about 5% while the second term contributes about 95% to the scale reference $m^2_{t\bar{t}}$. The cross section for that bin is expected to be lower compared to the same cross section for massless quarks, which provides the sensitivity to the running mass $m_t(\mu = m_{t\bar{t}})$. Figure 9 (right) shows the extracted running mass, based on the mass dependent cross sections and with the predictions evaluated at the scale given by $m_{t\bar{t}}$ for each bin. The masses are presented as a ratio to the reference mass used in the evaluation of the running as indicated on the figure (the 3rd data point). The measurements are consistent with the QCD prediction for the running of the top quark mass shown by the red shaded area.

With a machine like FCC-hh with an expected cms energy of 100 TeV for pp collisions a much larger reach in scale $m_{t\bar{t}}$ up to O(10) TeV is expected.

A study of production of radiative top anti-top quark pairs in e^+e^- annihilation at future linear colliders showed sensitivity to the running top quark mass [36]. When an energetic photon with energy E_γ is emitted in the process $e^+e^- \to t\bar{t}\gamma$ at cms energy $\sqrt{s}$ the effective cms energy of the $t\bar{t}$ system is $s' = s\sqrt{1-2E_\gamma/s}$. Figure 10 (left) shows the result of a detailed simulation study for the CLIC linear collider proposal for a cms energy of $\sqrt{s} = 380$ GeV. The simulated data for the event rate as a function of the effective cms energy $\sqrt{s'}$ shows the onset of $t\bar{t}$ production at the threshold and then a rising event rate with increasing $\sqrt{s'}$. The top quark mass dependence is studied for a scenario with $\sqrt{s} = 500$ GeV in four bins of $\sqrt{s'}$. The mass is extracted in the MSR scheme as a function of the scale parameter R, which is related to the top quark 3-momenta [36]. The second data point, which corresponds to the first bin after the bin containing the threshold region, already shows a significantly lower top quark mass. The second data point based on the range $[374, 411]$ GeV is already within reach of the CLIC scenario with $\sqrt{s} = 380$ GeV.

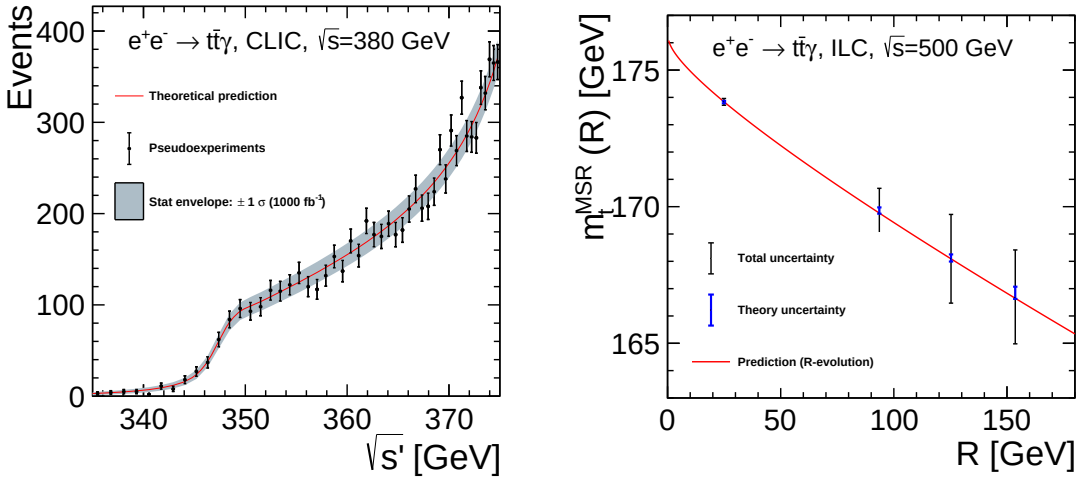

Figure 10: (left) The figure shows predictions for the number of radiative $t\bar{t}\gamma$ events per bin in $\sqrt{s'}$ in a CLIC scenario with data taken at $\sqrt{s} = 380$ GeV. (right) The figure shows the extracted top quark mass $m_t^{MSR}(R)$ for an ILC simulation at $\sqrt{s} = 500$ GeV in the MSR scheme as function of scale parameter R. The prediction for the running top quark mass is given by the red line [36].

Measurements of the mass of the b quark $m_b(Q)$ at large energy scales Q have been performed since large samples of Z boson decays to b quark pairs became available with the LEP and SLC experiments, see e.g. [12]. In these analyses the ratios of 3-jet fractions are measured in Z boson decays to b-jets and light quark jets. The measurements are compared to NLO QCD predictions with full quark mass dependence in order to extract the b quark mass at the Z boson mass scale in the $\overline{MS}$ scheme $m_b(m_Z) = (2.90 \pm 0.31)$ GeV [12, 37]. Compared to the PDG average for the b quark mass at low scales in the $\overline{MS}$ scheme $m_b(m_b) = (4.18^{+0.04}_{-0.03})$ GeV there is already evidence at almost four standard deviations for a running b quark mass.

A new method to measure the b quark mass at the scale of the Higgs boson mass $m_b(m_H)$ was introduced in [37]. The branching ratio for Higgs boson decays to a pair of b quarks $\Gamma(H \to b\bar{b}) \sim m_b(m_H)^2$ in the standard model. In order to use measurements by the LHC experiments ATLAS and CMS with reduced experimental uncertainties the ratio $\Gamma(H \to b\bar{b})/\Gamma(H \to ZZ)$ is used. This

analysis finds $m_b(m_H) = (2.60^{+0.36}_{-0.31})$ GeV, where the uncertainties are limited by the experimental errors. In the SM in leading order the b quark mass m_b and the b quark Yukawa coupling to the Higgs boson y_b are related by $y_b = m_b/(2VEV_H)$ and thus this measurement assumes the SM value for y_b [37]. All current measurements of $m_b(Q)$ are shown in figure 11 (left) and compared with the QCD prediction for the running b quark mass [37].

Future prospects for such measurements are discussed in [38]. The measurement of $m_b(m_Z)$ from the ratio of 3-jet rates in Z boson decays to b and light jets is estimated to have an uncertainty of about 120 MeV [39]. This assumes a large sample of Z boson decays at a future e^+e^- collider and theoretical improvements including NNLO QCD predictions with full mass effects for 3-jet production in Z boson decays. A new study considers the dependence on $m_b(m_Z)$ of the EWPO derived from Z boson decays $\Gamma(Z \to b\bar{b})$, $\mathrm{BR}(Z \to b\bar{b})$ and $R_{0,b} = \Gamma(Z \to b\bar{b})/\Gamma(Z \to hadrons)$ [40]. It is found that based on the predictions for measurements of the EWPO with FCC-ee [2] a precision for $m_b(m_Z)$ of about 5% or 140 MeV could be obtained. The future prospects are summarised in figure 11 (right) [38]. The measurement based on Z boson EWPO is referred to as "GigaZ Z-decays" while the measurement based on the 3-jet rates ratio is referred to as "GigaZ 3-jets". The figure also shows expectations for improved measurements of the ratio $\Gamma(H \to b\bar{b})/\Gamma(H \to ZZ)$ with HL-LHC or a Higgs factory. These expectations also assume theory progress for the calculation of electro-weak corrections up to NNLO. With the precision of these expected measurements new stringent tests of the SM become possible.

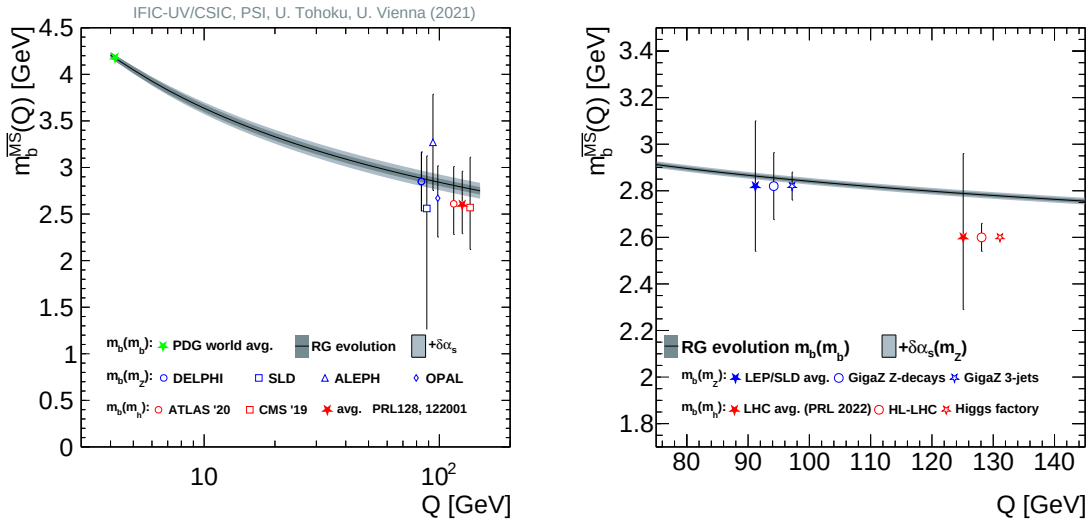

Figure 11: (left) The figure shows measurements of the b quark mass $m_b^{\overline{MS}}(Q)$ as function of the scale Q by various groups as indicated. Superimposed as line and band is the QCD prediction for the running b quark mass with uncertainties [37]. (right) The figure shows averages of the measurements shown on the left together with estimates for measurements in future programs. The line and band shows the prediction for the running b quark mass with uncertainties [38].

8. ep colliders

The first electron proton (ep) collider was the HERA machine operated by DESY in Hamburg, Germany, from 1990 to 2007. The HERA program yielded many important results for tests of QCD, measurements of the strong coupling constant and structure of the proton in high energy interactions, see e.g. [41]. The determination of the parton density functions (pdf) of the proton at HERA is together with other measurements an essential foundation of predictions for LHC experiments, see e.g. [42].

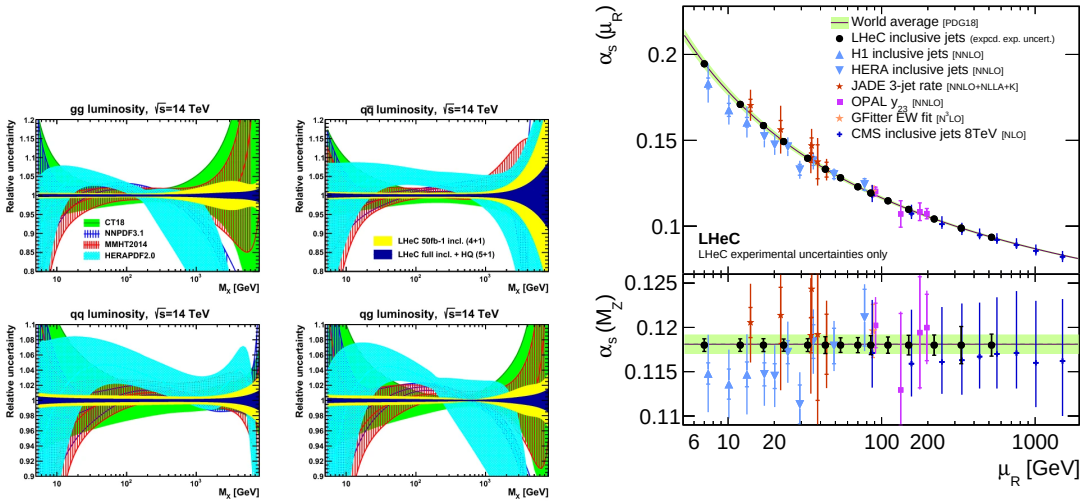

Figure 12: (left) The figure shows determinations of parton-parton luminosities for the production of a heavy particle of mass M_X from several pdf fits as indicated. Superimpoosed are predictions for the same luminosities based on the LHeC proposal in yellow and dark blue [43, 44]. (right) The figure shows determinations of $\alpha_s(\mu_R)$ (converted to $\alpha_s(m_Z)$ in the lower plot) by various experiments and groups and the expectation for measurements from the LHeC program. The line and green band show the current world average with uncertainties [6].

The Large Hadron Electron Collider (LHeC) proposal [6, 44] addresses as one of its main objectives the determination of proton pdfs to very good accuracy for important kinematic regions of the LHC pp collisions. The LHeC adds an electron accelerator for electron energies of 50 to 60 GeV based on the energy recovery linac (ERL) technique to one of the interaction points of the LHC. The combination of a 7 TeV proton beam with a 50 (60) GeV electron beam results in cms energy of the ep collisions of 1.2 (1.3) TeV. This is well above the collision energy reached by HERA and opens up direct production of heavy particles such as Higgs bosons or top quarks in CC or NC DIS processes. The luminosity of the ep collisions is foreseen to reach $10^{34}/(cm^2 s)$ such that also rare processes are accessible.

Figure 12 (left) shows LHeC predictions for the parton luminosites, for parton interactions gg, $q\bar{q}$, qg and qq as indicated, for the production of a heavy object of mass M_X. The parton luminosities are a result of combining the contributions from the proton pdfs leading to the given parton scattering. The LHeC predictions, for two different data set sizes, are compared with contemporary pdf determinations based on HERA, LHC and other data. The large improvement in uncertainties at all mass scales, but in particular for low masses and for large masses, is clearly

visible. This would have important consequences for many analyses at LHC and for the upcoming HL-LHC program, since all studies currently limited by proton pdf uncertainties would improve directly.

Another important aspect of a LHeC program would be determinations of the strong coupling constant with uncertainties competitive with the best alternative methods [1]. The determination of $\alpha_s(m_Z)$ together with pdfs from the evolution of structure functions measured with LHeC DIS is predicted to reach an uncertainty of $\Delta\alpha_s(m_Z) = 0.00022$ [44]. When inclusive jet production is added to the structure function evolution the uncertainty is predicted as $\Delta\alpha_s(m_Z) = 0.00016$. These very precise measurements of $\alpha_s(m_Z)$ would further improve many HL-LHC analysis, and would serve to cross check the precise determinations of α_s at low energy scales by Lattice QCD methods. Figure 12 (right) [6] illustrates this by showing predicted measurements of $\alpha_s(\mu_R)$ at energy scale μ_R by the LHeC experiment. The predictions are compared with several existing measurements and the large improvement in predicted uncertainties is clearly visible.

9. Hadron hadron collisions

The LHC collider provides to the experiments very large and diverse data sets from production of jets at low transverse momenta to production of heavy bosons, heavy quarks, and jets at energy scales of O(1) TeV. There are many different studies of aspects of the strong interaction based on these data sets, see e.g. [45]. We select here just two examples with particular promise for improvements in the future.

9.1 Drell-Yan production

Drell-Yan (DY) production refers to the observation of opposite charge lepton pairs (electrons or muons in practice) in pp collisions. We describe here the DY process, because it allows an especially accurate determination of the strong coupling constant reflecting the very good experimental and theoretical control with data from high energy pp collisions at the LHC. The lepton pair is produced via the electroweak interaction and thus the prediction in the SM is inclusive in the QCD calculation. Figure 13 shows a representative Feynman diagram in electro-weak LO for the DY process at the parton level with an initial $q\bar{q}$ pair. The preceding production of the $q\bar{q}$ pair from the pp collision, which will depend on the proton pdfs, is not shown. QCD corrections are connected with gluon radiation from the initial partons.

The ATLAS collaboration has measured DY production with e^+e^- and $\mu^+\mu^-$ pairs using the LHC Run 2 data at $\sqrt{s} = 8$ TeV [46]. The measurement required lepton pairs with invariant mass $80 < m_{l\bar{l}} < 100$ GeV in order to select Z boson decays. The measurements are performed in ranges of lepton pair transverse momentum p_T and rapidity y and are extrapolated to the full phase space using a decomposition in polynomials in azimuth and polar angles. The SM predictions are available in N3LO with resummation of soft gluon contributions for low lepton pair p_T in N3LL and approximately in N4LL referred to as N4LLa. The predictions are coded in the program DYTurbo [47].

Figure 14 (left) shows predictions from DYTurbo performed by ATLAS for the p_T spectrum of the lepton pairs with a Z boson selection for different values of the strong coupling constant $\alpha_s(m_Z)$ for the full phase space. The plot shows that changes in $\alpha_s(m_Z)$ by about 10% translate to changes

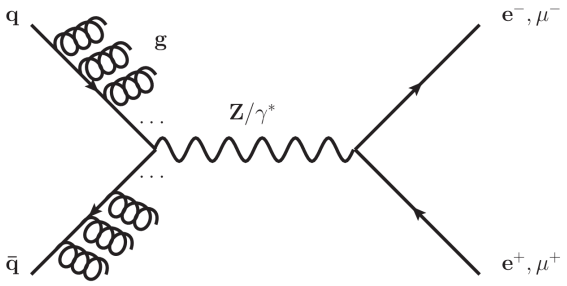

Figure 13: The figure shows the LO electro-weak Feynman diagram for $q\bar{q}$ annihilation to a lepton pair with gluon lines indicating QCD corrections [46].

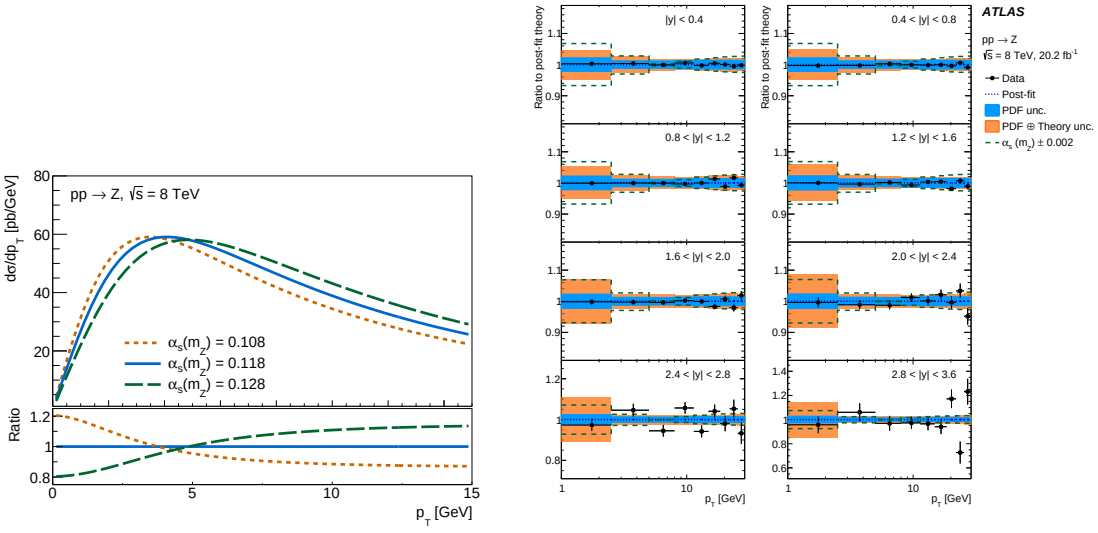

Figure 14: (left) The figure shows predictions in N3LO+N4LLa QCD calculated with DYTurbo for the p_t spectrum of DY production of Z bosons in pp collisions at 8 TeV. The lines show the predictions for different values of $\alpha_s(m_Z)$ as indicated. (right) The figure shows measurements of the DY cross section at 8 TeV as function of lepton pair p_t in bins of lepton pair rapidity y. The theory predictions are divided by the measurements. The shaded areas give the main uncertainties as indicated. The dashed lines correspond to variations of $\alpha_s(m_Z)$ in the predictions as indicated [46].

in the differential cross section of about the same size. Figure 14 (right) shows results of fits of the theory predictions to the data in ranges of p_T and rapidity y of the lepton pairs by ATLAS. The ratios of the data to the fitted theory show good agreement. The main uncertainties are indicated by the shaded areas as those from pdfs and the theory. The dashed lines for $\Delta\alpha_s(m_Z) = 0.002$ indicate the sensitivity of the measurements. Other uncertainties are connected with the model for non-perturbative effects, and experimental effects.

The main result can be presented as

$$\begin{aligned} \alpha_s(m_Z) &= 0.11828 \pm 0.00044_{exp.} \pm 0.00051_{pdf}{}^{+0.00012}_{-0.00020}{}_{non-pert} \pm {}^{+0.00061}_{-0.00057}{}_{theo.} \\ \alpha_s(m_Z) &= 0.11828 \pm 0.00090 \ , \end{aligned} \tag{8}$$

where all uncertainties connected with the theory prediction are added in quadrature to obtain the

"theo." uncertainty. If the only approximately known N4LLa part of the prediction is replaced by the fully known N3LL terms the result changes to $\alpha_s(m_Z) = 0.1187 \pm 0.0010$ due to an increase of the scale uncertainty from ± 0.00042 to ± 0.00066. The pdf uncertainty is obtained by propagating the uncertainties of the pdf set into the fit. The dependence of the pdfs on α_s is parametrised in the pdf sets and taken into account of in the fits.

Further tests were done in order to validate this result. A simultaneous optimisation of the proton pdfs and the fit to the lepton pair p_T distributions gives $\alpha_s(m_Z) = 0.11866 \pm 0.00064_{fit}$ which is consistent with main result. In total four different pdf sets determined in N3LO were used in fits based on N3LO+N3LL predictions and the results cover a range of $\Delta\alpha_s(m_Z) = \pm 0.001$. This is larger by a factor of two than the individual pdf uncertainty but consistent with the total uncertainty found for N3LO+N3LL fits (see above).

The measurement is as precise as the PDG world average $\alpha_s(m_Z) = 0.1180 \pm 0.0009$ [8] and its total errors are dominated by theory and pdf related uncertainties.

9.2 Di-jets

The production of two jets in pp collisions can be interpreted as probing fundamental parton parton interactions mediated by strong interactions. The fundamental interactions are between gg, qg, qq and $q\bar{q}$ pairs, see also section 8. In the ATLAS analysis [48] angular distributions of high transverse momentum jets are measured with 13 TeV data. The jets are reconstructed with the anti-kt algorithm with a radius $R = 0.4$, and $p_{t,jet1} > 440$ GeV and $p_{t,jet2} > 60$ GeV, for the two largest-p_t jets. The angular variable $\chi = \cot\theta^* \approx \exp(y_1 - y_2)$ with rapidities y_i of the two selected jets is introduced. The distributions of χ are measured for $|y^*| = |y_1 - y_2|/2 < 1.7$ and $|y_B| = |y_1 + y_2|/2 < 1.1$ in bins of the di-jet invariant masses m_{jj}. The di-jet invariant masses set the scale of the interactions from 3.4 TeV to more than 5.4 TeV.

Figure 15 presents the results from ATLAS together with predictions based on simulated event samples reweighted to NLO QCD predictions and corrected for small electro-weak corrections [48]. The distributions of the predictions are normalised to the data in each bin of m_{jj}. The predictions agree well with the data, confirming the validity of QCD with its assumptions of pointlike partons up to energy scales of about 5 TeV. The figure also shows expectations from models of contact interactions (CI) for two values corresponding to the mass of a hypothetical exchanged particle. These models predict deviations from the SM predictions at large scales m_{jj}.

Studies of this kind are expected to reach much higher energy scales $m_{jj} \approx 40$ TeV at FCC-hh, by scaling the current reach of LHC analyses to the FCC-hh cms energy of 100 TeV. If no new interactions are found quarks would be shown as pointlike down to length scales of $2.5 \cdot 10^{-6}$ fm.

10. Summary

We view results discussed in the summary through the lens of the precision in the determination of the strong coupling constant achieved so far and the prospects for improvements in the future. Figure 16 from [46] gives an overview of determinations of $\alpha_s(m_Z)$ of which the majority was discussed here. The various groups of measurements have currently about the same precision, with the notable exceptions of measurements based on Lattice QCD and from the Z boson p_t spectrum

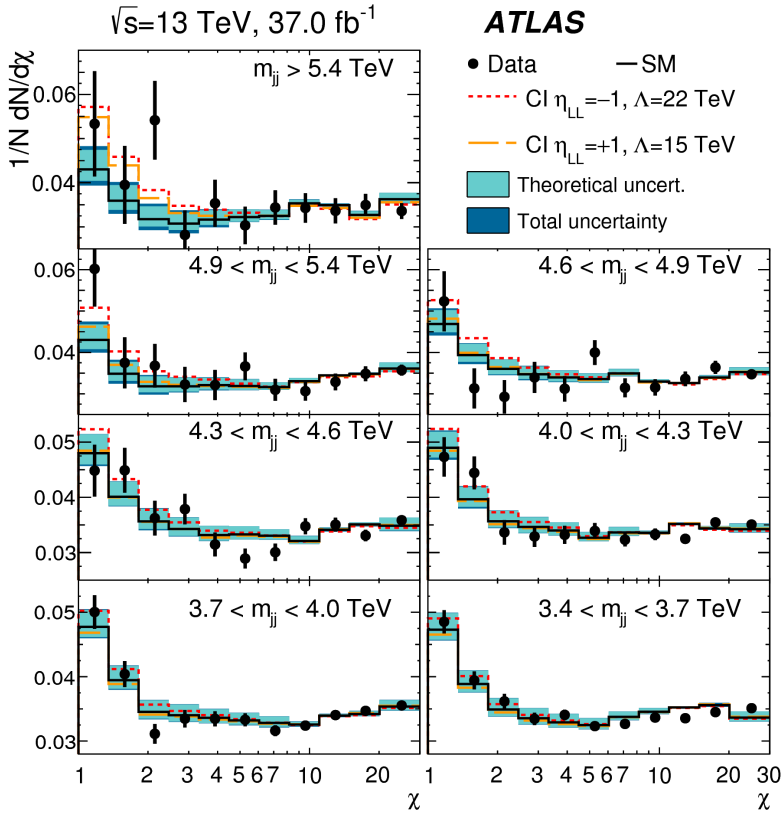

Figure 15: The figure shows the distribution of the angular observable χ for di-jet events in pp collisions at 13 TeV in bins of di-jet invariant mass m_{jj} by ATLAS. Superimposed as lines and bands are QCD predictions with uncertainties and as dotted and dashed lines expectations for hypothetical contact interactions at high scales as indicated [48].

by ATLAS, see section 9.1. All measurements are discussed in [1]. The world average shown does not contain the new results from ATLAS. The precision for $\alpha_s(m_Z)$ is now well below 1%.

In table 1 we collect the measurement labels from figure 16 and add the estimates from [1] about their future prospects possibly connected with a proposed future collider project.

One pattern that emerges in the predictions is that inclusive measurements can lead to uncertainties $\Delta\alpha_s(m_Z) \approx 0.1\%$ (Electro-weak fit, DIS structure functions), the best uncertainties for semi-inclusive observables are $\Delta\alpha_s(m_Z) \approx 1\%$ (LHC Z p_t, fragmentation functions) while for exclusive observables uncertainties are predicted as $\Delta\alpha_s(m_Z) \geq 1\%$ (Jets, event shapes at LHC or in e^+e^-). Together with determinations of $\alpha_s(m_Z)$ from Lattice QCD, which is predicted to benefit from theory progress, measurements from selected inclusive observables are expected to yield the most precise values for the strong coupling constant. These measurements would be made possible by the proposed future collider programs LHeC, FCC-ee and FCC-eh. For the measurements of top quark properties and studies of the running of the top quark mass the FCC-ee (or a linear collider) and the FCC-hh will be essential.

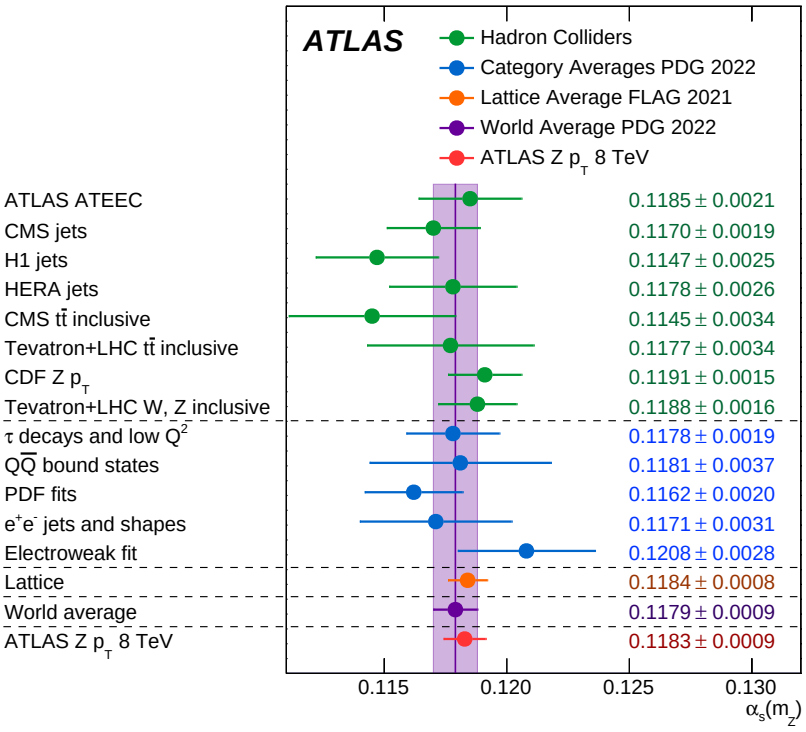

Figure 16: The figure shows determinations of $\alpha_s(m_Z)$ by various groups and observables. The colour code groups the determinations in categories as indicated. The results from Lattice QCD, the world average and the results from the ATLAS analysis of the Z boson p_t spectrum in DY production are shown separately [46].

Categories from fig. 16		expected $\Delta\alpha_s(m_Z)$
Hadron colliders	ATLAS ATEEC CMS jets H1 jets HERA jets CMS $t\bar{t}$ inclusive Tevatron+LHC $t\bar{t}$ inclusive CDF Z p_T Tevatron+LHC W, Z inclusive	$< 1.5\%$ (theory, pdfs, future ep collider)
Category averages PDG 2022	τ decays and low Q^2	$< 1\%$ (theory, spectral functions)
	$Q\bar{Q}$ bound states	1.5% (theory)
	PDF fits	0.2% (future ep collider)
	e^+e^- jets and shapes	1% (theory)
	Electroweak fit	0.1% (future e^+e^- collider)
	Lattice	0.1% (theory)
	ATLAS Z p_T 8 TeV	$< 1\%$ (theory, pdfs)

Table 1: The table shows for the determinations of $\alpha_s(m_Z)$ in the categories from figure 16 the evaluations for expected uncertainties $\Delta\alpha_s(m_Z)$ with proposed future collider programs or other improvements as indicated in brackets [1].

References

[1] D. d'Enterria et al., *The strong coupling constant: State of the art and the decade ahead*, 2203.08271.

[2] FCC collaboration, *FCC Physics Opportunities: Future Circular Collider Conceptual Design Report Volume 1*, *Eur. Phys. J. C* **79** (2019) 474.

[3] CEPC Study Group collaboration, *CEPC Conceptual Design Report: Volume 1 - Accelerator*, 1809.00285.

[4] CEPC Study Group collaboration, *CEPC Conceptual Design Report: Volume 2 - Physics & Detector*, 1811.10545.

[5] ILC collaboration, H. Baer et al., eds., *The International Linear Collider Technical Design Report - Volume 2: Physics*, 1306.6352.

[6] LHeC, FCC-he Study Group collaboration, *The Large Hadron–Electron Collider at the HL-LHC*, *J. Phys. G* **48** (2021) 110501 [2007.14491].

[7] G. Bernardi et al., *The Future Circular Collider: a Summary for the US 2021 Snowmass Process*, 2203.06520.

[8] Particle Data Group collaboration, *Review of Particle Physics*, *PTEP* **2022** (2022) 083C01.

[9] B. Dehnadi, A.H. Hoang, O.L. Jin and V. Mateu, *Top quark mass calibration for Monte Carlo event generators — an update*, *JHEP* **12** (2023) 065 [2309.00547].

[10] ALEPH, DELPHI, L3, OPAL, SLD, LEP Electroweak Working Group, SLD Electroweak Group, SLD Heavy Flavour Group collaboration, *Precision electroweak measurements on the Z resonance*, *Phys. Rept.* **427** (2006) 257 [hep-ex/0509008].

[11] OPAL collaboration, *Charged particle momentum spectra in e+ e- annihilation at s**(1/2) = 192-GeV to 209-GeV*, *Eur. Phys. J. C* **27** (2003) 467 [hep-ex/0209048].

[12] S. Kluth, *Tests of Quantum Chromo Dynamics at e+ e- Colliders*, *Rept. Prog. Phys.* **69** (2006) 1771 [hep-ex/0603011].

[13] Y.L. Dokshitzer, V.A. Khoze, A.H. Mueller and S.I. Troian, *Basics of perturbative QCD*, Editions Frontières (1991).

[14] C.P. Fong and B.R. Webber, *One and two particle distributions at small x in QCD jets*, *Nucl. Phys. B* **355** (1991) 54.

[15] CDF collaboration, *Momentum Distribution of Charged Particles in Jets in Dijet Events in $p\bar{p}$ Collisions at $\sqrt{s}$ = 1.8 TeV and Comparisons to Perturbative QCD Predictions*, *Phys. Rev. D* **68** (2003) 012003.

[16] Y.L. Dokshitzer, V.A. Khoze and S.I. Troian, *Particle spectra in light and heavy quark jets*, *J. Phys. G* **17** (1991) 1481.

[17] Y.L. Dokshitzer, V.A. Khoze and S.I. Troian, *On specific QCD properties of heavy quark fragmentation ('dead cone')*, *J. Phys. G* **17** (1991) 1602.

[18] S. Kluth, W. Ochs and R. Perez Ramos, *Observation of the dead cone effect in charm and bottom quark jets and its QCD explanation*, *Phys. Rev. D* **107** (2023) 094039 [2303.13343].

[19] V.A. Khoze, W.J. Stirling and L.H. Orr, *Soft gluon radiation in e+ e- —> t anti-t*, *Nucl. Phys. B* **378** (1992) 413.

[20] G.P. Salam, *Towards Jetography*, *Eur. Phys. J. C* **67** (2010) 637 [0906.1833].

[21] D.E. Soper, *Basics of QCD perturbation theory*, in *24th Annual SLAC Summer Institute on Particle Physics: The Strong Interaction, From Hadrons to Protons*, pp. 15–42, 8, 1996 [hep-ph/9702203].

[22] V. Del Duca, C. Duhr, A. Kardos, G. Somogyi and Z. Trócsányi, *Three-Jet Production in Electron-Positron Collisions at Next-to-Next-to-Leading Order Accuracy*, *Phys. Rev. Lett.* **117** (2016) 152004 [1603.08927].

[23] A. Gehrmann-De Ridder, T. Gehrmann, E.W.N. Glover and G. Heinrich, *NNLO corrections to event shapes in e+ e- annihilation*, *JHEP* **12** (2007) 094 [0711.4711].

[24] S. Weinzierl, *Event shapes and jet rates in electron-positron annihilation at NNLO*, *JHEP* **06** (2009) 041 [0904.1077].

[25] A.H. Hoang, D.W. Kolodrubetz, V. Mateu and I.W. Stewart, *Precise determination of α_s from the C-parameter distribution*, *Phys. Rev. D* **91** (2015) 094018 [1501.04111].

[26] P. Nason and G. Zanderighi, *Fits of α_s using power corrections in the three-jet region*, *JHEP* **06** (2023) 058 [2301.03607].

[27] G. Bell, C. Lee, Y. Makris, J. Talbert and B. Yan, *Effects of Renormalon Scheme and Perturbative Scale Choices on Determinations of the Strong Coupling from e^+e^- Event Shapes*, 2311.03990.

[28] X. Chen, T. Gehrmann, E.W.N. Glover, A. Huss and J. Mo, *NNLO QCD corrections in full colour for jet production observables at the LHC*, *JHEP* **09** (2022) 025 [2204.10173].

[29] D. Britzger et al., *NNLO interpolation grids for jet production at the LHC*, *Eur. Phys. J. C* **82** (2022) 930 [2207.13735].

[30] B. Naroska, *e^+e^- Physics with the JADE Detector at PETRA*, *Phys. Rept.* **148** (1987) 67.

[31] FCC collaboration, *FCC-ee: The Lepton Collider: Future Circular Collider Conceptual Design Report Volume 2*, *Eur. Phys. J. ST* **228** (2019) 261.

[32] A.V. Nesterenko, *Electron–positron annihilation into hadrons at the higher-loop levels*, *Eur. Phys. J. C* **77** (2017) 844 [1707.00668].

[33] OPAL collaboration, *Measurement of alpha(s) with Radiative Hadronic Events*, *Eur. Phys. J. C* **53** (2008) 21 [0902.1128].

[34] J.A.M. Vermaseren, S.A. Larin and T. van Ritbergen, *The four loop quark mass anomalous dimension and the invariant quark mass*, *Phys. Lett. B* **405** (1997) 327 [hep-ph/9703284].

[35] CMS collaboration, *Running of the top quark mass from proton-proton collisions at* $\sqrt{s}$ = *13TeV*, *Phys. Lett. B* **803** (2020) 135263 [1909.09193].

[36] M. Boronat, E. Fullana, J. Fuster, P. Gomis, A. Hoang, V. Mateu et al., *Top quark mass measurement in radiative events at electron-positron colliders*, *Phys. Lett. B* **804** (2020) 135353 [1912.01275].

[37] J. Aparisi et al., *mb at mH: The Running Bottom Quark Mass and the Higgs Boson*, *Phys. Rev. Lett.* **128** (2022) 122001 [2110.10202].

[38] J. Aparisi et al., *Snowmass White Paper: prospects for measurements of the bottom quark mass*, 2203.16994.

[39] J. Fuster, A. Irles, G. Rodrigo, S. Tairafune, M. Vos, H. Yamamoto et al., *Prospects for the measurement of the b-quark mass at the ILC*, in *International Workshop on Future Linear Colliders*, 4, 2021 [2104.09924].

[40] S. Kluth, $m_{\mathrm{b}}(m_{\mathrm{Z}^0})$*revisited with Zedometry*, *Eur. Phys. J. C* **82** (2022) 240 [2201.02417].

[41] C. Diaconu, T. Haas, M. Medinnis, K. Rith and A. Wagner, *Physics Accomplishments of HERA*, *Ann. Rev. Nucl. Part. Sci.* **60** (2010) 101.

[42] PDF4LHC Working Group collaboration, *The PDF4LHC21 combination of global PDF fits for the LHC Run III*, *J. Phys. G* **49** (2022) 080501 [2203.05506].

[43] S. Amoroso et al., *Snowmass 2021 Whitepaper: Proton Structure at the Precision Frontier*, *Acta Phys. Polon. B* **53** (2022) 12 [2203.13923].

[44] K.D.J. André et al., *An experiment for electron-hadron scattering at the LHC*, *Eur. Phys. J. C* **82** (2022) 40 [2201.02436].

[45] T. Gehrmann and B. Malaescu, *Precision QCD Physics at the LHC*, *Ann. Rev. Nucl. Part. Sci.* **72** (2022) 233 [2111.02319].

[46] ATLAS collaboration, *A precise determination of the strong-coupling constant from the recoil of Z bosons with the ATLAS experiment at* $\sqrt{s}$ = 8 *TeV*, 2309.12986.

[47] S. Camarda et al., *DYTurbo: Fast predictions for Drell-Yan processes*, *Eur. Phys. J. C* **80** (2020) 251 [1910.07049].

[48] ATLAS collaboration, *Search for new phenomena in dijet events using 37 fb^{-1} of pp collision data collected at $\sqrt{s}$ =13 TeV with the ATLAS detector*, *Phys. Rev. D* **96** (2017) 052004 [1703.09127].